TU Delft

Delft University of Technology

Dynamic operation of water electrolyzers

A review for applications in photovoltaic systems integration

Martinez Lopez, V.A.; Ziar, H.; Haverkort, J.W.; Zeman, M.; Isabella, O.

DOI
10.1016/j.rser.2023.113407

Publication date
2023

Document Version
Final published version

Published in
Renewable and Sustainable Energy Reviews

Citation (APA)
Martinez Lopez, V. A., Ziar, H., Haverkort, J. W., Zeman, M., & Isabella, O. (2023). Dynamic operation of water electrolyzers: A review for applications in photovoltaic systems integration. *Renewable and Sustainable Energy Reviews*, *182*, Article 113407. https://doi.org/10.1016/j.rser.2023.113407

Important note
To cite this publication, please use the final published version (if applicable).
Please check the document version above.

Copyright
Other than for strictly personal use, it is not permitted to download, forward or distribute the text or part of it, without the consent of the author(s) and/or copyright holder(s), unless the work is under an open content license such as Creative Commons.

Takedown policy
Please contact us and provide details if you believe this document breaches copyrights.
We will remove access to the work immediately and investigate your claim.

This work is downloaded from Delft University of Technology.
For technical reasons the number of authors shown on this cover page is limited to a maximum of 10.

Renewable and Sustainable Energy Reviews 182 (2023) 113407

Contents lists available at ScienceDirect

Renewable and Sustainable Energy Reviews

journal homepage: www.elsevier.com/locate/rser

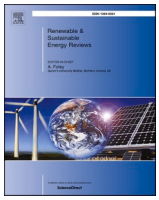

Dynamic operation of water electrolyzers: A review for applications in photovoltaic systems integration

V.A. Martinez Lopez [a,*], H. Ziar [a], J.W. Haverkort [b], M. Zeman [a], O. Isabella [a]

[a] Delft University of Technology, Photovoltaic Materials and Devices, Mekelweg 4, 2628CD, Delft, the Netherlands
[b] Delft University of Technology, Process & Energy Department, Leeghwaterstraat 39, 2628CB, Delft, the Netherlands

A B S T R A C T

This review provides a comprehensive overview of the dynamics of low-temperature water electrolyzers and their influence on coupling the three major technologies, alkaline, Proton Exchange Membrane (PEM) and, Anion Exchange Membrane (AEM) with photovoltaic (PV) systems. Hydrogen technology is experiencing considerable interest as a way to accelerate the energy transition. With no associated CO_2 emissions and fast response, water electrolyzers are an attractive option for producing *green* hydrogen on an industrial scale. This can be seen by the ambitious goals and large-scale projects being announced for hydrogen, especially with solar energy dedicated entirely to drive the process. The electrical response of water electrolyzers is extremely fast, making the slower variables, such as temperature and pressure, the limiting factors for variable operation typically associated with PV-powered electrolysis systems. The practical solar-to-hydrogen efficiency of these systems is in the range of 10% even with a very high coupling factor exceeding 99% for directly coupled systems. The solar-to-hydrogen efficiency can be boosted with a battery, potentially sacrificing the cost. The intermittency of solar irradiance, rather than its variability is the biggest challenge for PV-hydrogen systems regarding operation and degradation.

1. Introduction

Hydrogen production with electricity is now in the spotlight as the world moves towards 2050 with net-zero emissions. This gas is so important in this energy transition that the International Energy Agency (IEA) has included it in its Net Zero Emission roadmap as playing a critical role [1]. To mention a few figures, it is expected that by 2030 the world will see 15 million hydrogen cars, and by 2050 the shipping industry will depend on hydrogen as its dominant fuel [1].

Nowadays, most of the hydrogen in the world is produced by Steam Methane Reforming (SMR), which consists of processing natural gas or coal with water vapor at elevated temperatures and pressure over nickel-alumina catalysts. The result is hydrogen gas and CO [2]. This process is CO_2 intensive (*grey hydrogen)*. Thus, if this method is to be used, a great effort must be focused on reducing the carbon footprint of grey hydrogen by using carbon sequestration (*blue hydrogen)* [2].

A better alternative is water electrolysis. The process will be explained in detail in the following sections. If the electricity source for electrolysis comes from renewable energy, the produced hydrogen will have no associated CO_2 emissions (*green hydrogen)*. Currently, electrolysis accounts only for 2% of the hydrogen production in the world, while most of it is a by-product of the chlor-alkali process [3]. Of all the processes primarily aiming at producing hydrogen, only 0.1% of all the hydrogen comes from water electrolysis as this technology still faces higher costs; further, the amount of electricity needed to turn from grey to green hydrogen is enormous, reaching the Terawatt-hour range [3] easily.

Many large-scale green hydrogen projects are being announced, such as a 150 million EUR investment project in Spain started in 2021 to power a 20 MW electrolyzer with solar energy. The produced hydrogen will be used as feedstock for ammonia production [4]. This highlights the importance of renewable hydrogen production in the near future. This is even enhanced by the fact that key oil-producing countries are also investing in hydrogen. A 5 billion USD project has been recently announced in Saudi Arabia, one of the leading oil producers in the world, to produce hydrogen entirely from renewable sources. It is expected that by 2030, the cost of hydrogen produced by this project will be lower than that of fossil-based production methods [5], which account for 830 million tons of CO_2 emitted per year [3].

The International Energy Agency (IEA) has compiled a database with large-scale electrolysis projects [6]. Fig. 1(a) shows the worldwide distribution of operational and under construction projects that will produce hydrogen powered exclusively from renewable sources (i.e. they do not depend on the grid nor are supporting the grid to absorb an excess of renewable production). The main renewable sources to produce the electricity for hydrogen production is onshore wind and solar PV as seen in Fig. 1(c).

* Corresponding author.
E-mail address: V.A.MartinezLopez@tudelft.nl (V.A. Martinez Lopez).

https://doi.org/10.1016/j.rser.2023.113407
Received 30 September 2022; Received in revised form 11 May 2023; Accepted 24 May 2023
Available online 31 May 2023
1364-0321/© 2023 The Authors. Published by Elsevier Ltd. This is an open access article under the CC BY license (http://creativecommons.org/licenses/by/4.0/).

List of symbols

T_{amb}	Ambient temperature [K]
A	Area [m^2]
k_B	Boltzmann constant 1.380649 × 10^{-23} [m^2 kg s^{-2} K^{-1}]
C	Capacitance [F]
E_{cell}	Cell voltage [V]
α	Charge transfer coefficient [−]
σ	Conductivity [Ω^{-1} m]
κ_0	Conductivity of the liquid [S/m]
I	Current [A]
j	Current density [A m^{-2}]
κ_{eff}	Effective conductivity [S/m]
e	Elementary charge [C]
ΔH	Enthalpy change [J mol^{-1}]
ΔS	Entropy change [J K^{-1} mol^{-1}]
$c_{ox,0}$	Equilibrium concentration of oxidant [mol/m^3]
$c_{red,0}$	Equilibrium concentration of reductant [mol/m^3]
j_0	Exchange current density [A m^{-2}]
F	Faraday's constant 96485.33 [C mol^{-1}]
Q_{gen}	Generated Heat flow [J s^{-1}]
ΔG	Gibbs free energy change [J mol^{-1}]
$\dot{h}_2$	Hydrogen flow [mol s^{-1}]
c_{ox}	Local concentration of oxidant [mol/m^3]
c_{red}	Local concentration of reductant [mol/m^3]
Q_{loss}	Loss to ambient Heat flow [J s^{-1}]
N_c	Number of electrolyzer cells [−]
n	Number of moles [mol]
η	Overpotential [V]
ε	Porosity [−]
E_{rev}	Reversible voltage [V]
S	Solar irradiance [W/m^2]
E^0	Standard potential [V]
V_0	Starting point voltage [V]
V_∞	Steady-state voltage [V]
b	Tafel slope [V]
T	Temperature [K]
C_t	Thermal Capacitance [J K^{-1}]
R_t	Thermal resistance [K W^{-1}]
E_{tn}	Thermoneutral voltage [V]
l	Thickness [m]
t	Time [s]
τ	Time constant [s]
τ	Tortuosity [−]
R	Universal gas constant 8.3144 [J K^{-1} mol^{-1}]
E	Voltage [V]
D_a	Ambipolar salt diffusion coefficient [m^2/s]
V	Volume [m^3]

Abbreviations

AEL	Alkaline Electrolyzer
AEM	Anion Exchange Membrane
AC	Alternating Current
I–V	Current-Voltage (curve)
DC	Direct Current
MEA	Membrane-Electrode Assembly
HTO	Hydrogen-To-Oxygen
PV	Photovoltaic
PTL	Porous Transport Layer
PEM	Proton Exchange Membrane
PEMEL	Proton Exchange Membrane Electrolyzer
R–C	Resistor-Capacitor
MPP	Maximum Power Point
MPPT	Maximum Power Point Tracker

These projects and roadmaps highlight the importance that hydrogen is experiencing during this energy transition. Successful integration of electrolyzers with the grid and highly variable renewable energy depends on the knowledge of the response of the electrolyzer plant to quick changes. This work provides extensive insight into the dynamic operation of low-temperature water electrolyzers, focusing on their integration with PV systems. Section 2 prnxovides the general background on water electrolysis and low-temperature electrolyzer technologies. Section 3 presents the dynamics of water electrolyzers, diving into the fast electrical response and the slower changes caused by temperature and pressure. The integration with solar energy is discussed in Section 4. This section contains all issues related to a dynamic operation, including lifetime concerns, and the conclusion is given in Section 5.

We want to highlight that our work focuses on the production of hydrogen as raw material and not on hydrogen for grid balancing or micro-grid applications as it is beyond our research goal. Although we included a brief discussion of the costs, an in-depth discussion is also outside of the scope as this topic might even deserve a literature review on its own.

2. Water electrolysis

Water electrolysis is an electrochemical process in which *electricity* (electro-) is used to *split* (-lysis) water molecules into dissolved oxygen and hydrogen. Concretely, this electrochemical process involves reduction-oxidation (redox) chemical reactions. Electrons will be produced (*ox*idation) at one *anode* and consumed (*red*uction) at the *cathode*.

The reactions occurring at each electrode will depend on whether the electrolyte is acidic or alkaline. They are summarized in Table 1.

Regardless of the electrolyte type, the overall reaction of water electrolysis can be written as

$$2H_2O(l) \rightarrow 2H_2(g) + O_2(g) \quad (1)$$

so for each 2 mol or molecules of water, the same amount of hydrogen and half this amount of oxygen is produced [8]. The addition "(g)" or "(l)" indicates that the products or reactants are in the gas or liquid phase, respectively.

Water electrolysis does not occur spontaneously for temperatures below 2250 °C [9]. It needs to be supplied with additional energy in the form of electricity and heat. The enthalpy of reaction is the change in enthalpy between reactants and products. When the products hydrogen and oxygen are produced in the gas-phase, this reads per mole of water (ΔH in [kJ mol^{-1}]) [9]:

$$\Delta H = \Delta G + T\Delta S \quad (2)$$

The enthalpy of reaction ΔH is associated with the entropy change of the environment and $T\Delta S$ with that of the system, the reactants and products in this case. The entropy of the reaction products, the gases oxygen and hydrogen, is higher than those of the liquid reactants, so $\Delta S > 0$.

The difference $-\Delta G$ is therefore associated with the overall entropy change. A spontaneous process is associated with an increase in entropy so that $\Delta G < 0$. Electrolysis is a non-spontaneous process, which requires work to be performed so that $\Delta G > 0$. The Gibbs free energy of reaction, ΔG, represents the maximum amount of work that can be performed by the energy released in the reaction in case $\Delta G < 0$ [9]. At standard conditions the change in Gibbs free energy is $\Delta G^0 = -237.2$ kJ/mol. This work may be supplied by applying a potential $E^0 = \Delta G^0/2F \approx 1.229$ V, called the standard electrode potential which is temperature

dependent, as seen in Equation (3) [10].

$$E^0 = 1.5184 - 1.5421 \times 10^{-3}T + 9.523 \times 10^{-5}T \ln T + 9.84 \times 10^{-8}T^2 \quad (3)$$

Thermodynamically, at least 1.229 V must be applied for reaction of Equation (1) to proceed [9].

With ΔG and ΔS both positive, the enthalpy of reaction is also positive, indicating an endothermic reaction. When additional heat surpassing $T\Delta S$ is supplied, cooling as avoided and the overall process becomes exothermic. Therefore, at potential equal to the thermoneutral voltage $E_{tn} = \Delta H/2F \approx 1.48$ V, there is no net heat production or consumption. Owing to energy losses due to resistance and irreversibility in the reaction, in practice usually a higher voltage is applied and the process will release heat [7–9]. These 'overpotentials' have different origins and are considered in more detail in Section 3.1.

2.1. Water electrolyzer technologies

Hydrogen can be produced at an industrial scale by applying the fundamentals of water electrolysis to large-scale electrolyzers. To do this, two technologies for low-temperature water electrolysis are commercially available and developed at industrial scales: alkaline and PEM. The AEM is the third low-temperature electrolysis technology and is still under development with only a few commercial products available.

2.1.1. Alkaline electrolyzer

Alkaline electrolyzers are the most mature electrolysis technology. The reactions are taking place in an alkaline electrolyte, so the equations of Table 1 (Alkaline row) are occurring.

The basic construction is shown in Fig. 2 (a). The electrodes, typically made of nickel or coated with Raney nickel as a catalyst at the cathode, are immersed in an *alkaline* solution (potassium or sodium hydroxide) with a typical concentration of 30 wt% and separated by a porous separator [9,11]. A mesh construction of the electrodes facilitates the removal of bubbles. The separator, which in the past was made of toxic asbestos but now is replaced by other materials such as a mixture of zirconium dioxide and polysulfone under the commercial name of Zirfon™, helps to keep the hydrogen and oxygen gases apart, preventing the formation of a dangerous combination of them [9]. This separator, however, must allow the transport of OH^- ions for the reaction to take place [9,11]. Adding this separator increases the cell's ionic resistance and facilitates the attachment of bubbles to it, leading to an increased electrical resistance caused by them [12]. If a gap exists between the electrodes and the separator, in this space bubbles will accumulate. The gap will influence how bubbles are aggregated, creating void spaces where no reaction occurs, thus, affecting the ohmic losses [12–15].

The freely moving bubbles impact the conductivity of the electrolyte by forcing the ions to take longer paths to reach the electrodes [15]. To overcome this problem, the electrodes can also be placed in the zero-gap configuration. Here, the electrodes are placed in direct contact with the separator. Although this helps to reduce the resistance caused by

Table 1
Reactions at electrodes depending on the electrolyte type (With information from Ref. [7])

Alkaline	Cathode	$2H_2O(l) + 2e^- \rightarrow H_2(g) + 2OH^-$
	Anode	$4OH^- \rightarrow 2H_2O(l) + O_2(g) + 4e^-$
Acidic	Cathode	$2H^+ + 2e^- \rightarrow H_2(g)$
	Anode	$2H_2O(l) \rightarrow 4H^+ + O_2(g) + 4e^-$

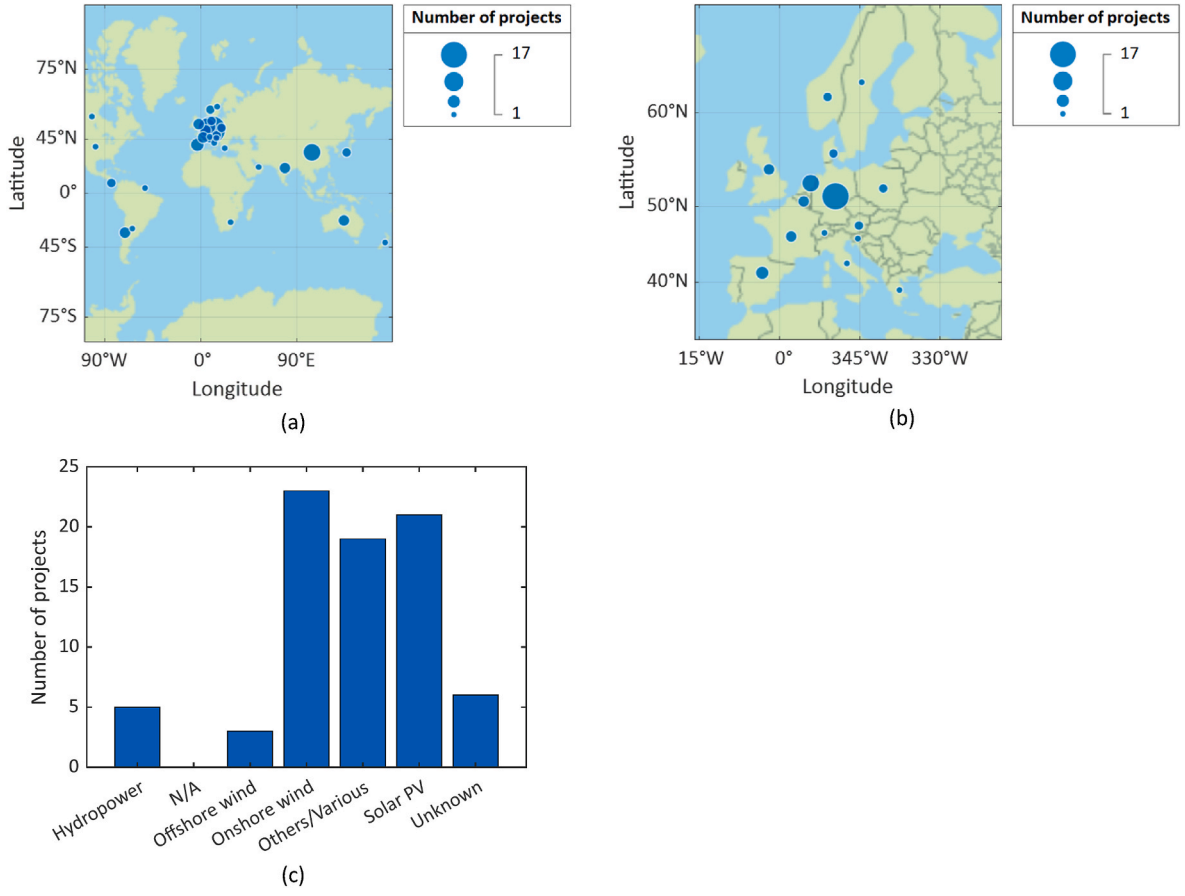

Fig. 1. (a) Worldwide distribution of electrolysis projects for hydrogen production. All these projects are either operational or under construction and are powered from dedicated renewable sources. (b) Zoom over Europe. (c) Renewable sources that power the electrolysis projects. With data from Ref. [6].

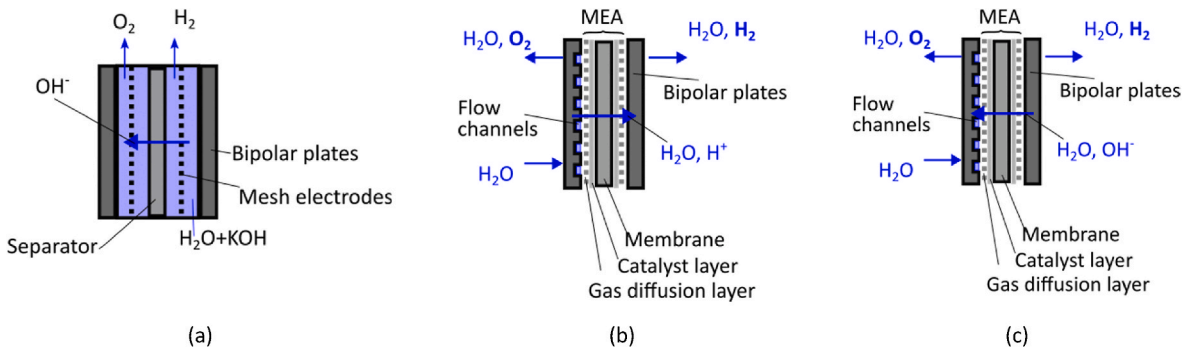

Fig. 2. (a) Construction and operation of an alkaline water electrolyzer. The electrodes and separator are immersed in an alkaline solution. The separator prevents the recombination of hydrogen and oxygen, which could lead to an explosion. At the same time, it allows the transport of OH^- ions needed to complete the reaction. Traditionally, a small gap (a few millimeters) existed between the electrodes and the separator, now usually removed in the zero-gap configuration where the electrodes are placed touching the separator. Electricity is supplied using the bipolar plates. (b) Construction and operation of a PEM water electrolyzer. The water is fed through the flow channels, which also help remove oxygen. Hydrogen H^+ ions and water molecules are transported through the Membrane-Electrode Assembly. This single-unit component consists of the porous electrodes, a catalyst layer, and the membrane. The electricity is supplied through the bipolar plates. (c) Construction and operation of an AEM water electrolyzer. Note that the construction is the same as the PEM electrolyzer. The main difference lays in the membrane. While PEM allows the movement of hydrogen H^+ ions, AEM allows the movement of hydroxyl ions, in the same way as the alkaline technology.

bubbles, it introduces other challenges for the separator, which needs to be well engineered to avoid gas crossover [9,16].

The alkaline technology consumes between 47 kWh and 66 kWh of electricity to produce 1 kg of hydrogen. In terms of percentage, this is equivalent to 50–68% (with respect to the lower, heating value of hydrogen, LHV = 33.33 kWh/kg) [17].

2.1.2. *Proton Exchange Membrane (PEM) electrolyzer*

An improvement to the alkaline technology was made in the era of the Gemini space program when a solid membrane replaced the liquid electrolyte of the fuel cells [18]. This new technology consists of a solid electrolyte that facilitates the use of the zero-gap configuration. The solid electrolyte is a thin polymer membrane that allows the conduction of ions [9,19]. Hence the name Polymer Electrolyte Membrane (PEM). Other names for this technology are Proton Exchange Membrane or Solid Polymer Electrolyte [19]. The material Nafion™, developed by DuPont, is one of the most well-known materials for the membrane [9, 20]. The presence of H^+ ions in the membrane causes it to be a very acidic medium that can corrode the elements in contact with it, namely, electrodes and catalyst layers [9]. The solution to prevent corrosion is using robust but often scarce materials in the electrodes and catalysts such as platinum and ruthenium, which result in elevated costs [9]. The reactions taking place in a PEM electrolyzer are described in Table 1 (Acidic row).

Another property of the membrane is its thickness. With 50–300 μm thickness, some design choices must be made. On the one hand, the membrane's thickness is related to this component's resistance. The thinner the membrane is, the lower the resistance. On the other hand, if a high-pressure operation is desired, the membrane must be thicker to prevent gas crossover and improve safety and Faraday efficiency [21]. An intermediate (catalyst) layer is introduced to facilitate the reaction. A gas diffusion layer is the last layer of this stack, which is pressed together to form a single unit called Membrane-Electrode Assembly or MEA [9] (see Fig. 2 (b)). The gas diffusion layer not only allows water into the cathode and facilitates the extraction of gases but also provides strength, allows compression, transports heat, and protects the catalysts from fluid flows.

In contact with the MEA are the bipolar plates where current is applied. They also contain flow channels to feed the water and facilitate the extraction of gases [9] (see Fig. 2 (b)). The bipolar plates also allow the connection of cells in series, forming a bipolar configuration. One plate receives the two terminals (hence the name), the positive of one cell and the negative of the next.

For industrial size units (around 1 MW), this technology and the alkaline have similar efficiencies (50–68% with respect to the LHV) [17]. The advantage of the PEM technology lays in a broader operating spectrum. While the minimum operating limit for the alkaline technology is set at 20% of its nominal capacity, PEM can go as low as 5%. On the other extreme, PEM, can operate beyond the nominal capacity, which is not possible for alkaline electrolyzers [17]. Another advantage of PEM is the ability to operate at higher current densities up to 2 A/m^2 (alkaline technology operates at a maximum of 0.8 A/m^2) [17]. This is translated in improved hydrogen production.

2.1.3. *Anion Exchange Membrane (AEM) Electrolyzer*

Anion-Exchange Membrane (AEM) electrolysis is an emerging technology that exploits the advantages of PEM electrolysis but operates in alkaline conditions. Hence, the reactions driving the process are also the alkaline row of Table 1.

Because of the alkaline environment, AEM does not need scarce materials such as iridium or platinum [16]. The AEM electrolyzer construction is similar to the PEM: a membrane sandwiched between two electrodes (see Fig. 2 (c)). The membrane allows the transport of hydroxyl-ions (OH^-) while keeping the product gases (hydrogen and oxygen) separated [22]. The difference with the alkaline technology is the separator. In the AEL, this is a porous material, while in AEM, the membrane is not. The membrane allows only the conduction of the OH^- ions and in the porous separator, these travel through the pores of the material [16]. The AEM electrolyzer can be fed pure, demineralized water as with PEM. However, the system's performance is poor due to the low availability of hydroxyl ions in the membrane [22], and it can lead to electrode degradation if fed exclusively to the anode [22,23]. A solution is to add an electrolyte, such as KOH, as done in AEL. The concentration of the electrolyte (typically 30% wt in AEL) can be reduced to 3–10% wt [23].

AEM is still a developing technology with chemical, mechanical and thermal stability challenges that ultimately lead to durability problems [16]. Research is also being conducted on membrane design, membrane-electrode assembly (MEA) construction, and electrocatalysts materials [16,23].

Despite still being in the developing phase, there are already commercial products based on AEM, such as the electrolyzers produced by HydroLite [24] or Enapter [25].

AEM still has lower efficiency than that of alkaline or PEM (67%, based on LHV for a unit size of a few kW) and combines characteristics of both. It can operate with the same maximum current density as a PEM (2 A/m^2) but cannot exceed the nominal capacity (same as alkaline technology) [17].

3. Dynamics of water electrolysis

The dynamic behavior impacts the development of control strategies for gas production. The stack's response depends on several factors, including water intake, temperature, and bubbles. Further, as these parameters are time-changing, the modeling can become very complex, making it unsuitable for control applications or very simplistic ignoring the time-varying parameters [26].

3.1. The voltage-current (I–V) characteristic

The starting point for understanding the operation of an electrolyzer is to recognize its polarization characteristics (I–V curve). In other words, how the voltage of the electrolyzer changes with the applied current under steady-state conditions. The voltage of an electrolysis cell (E_{cell}) is the sum of the reversible voltage and so-called overpotentials:

$$E_{cell} = E_{rev} + \eta_{act,an} + |\eta_{act,cat}| + \eta_{ohm} \quad (4)$$

The reversible potential, $E_{rev} = 1.23$ V at standard conditions, depends on pressure, temperature, and local reactant and product concentrations through the Nernst equation [8].

The extra voltage (overpotential) imposed by η_{act} and η_{ohm} constitute losses and depend on the applied current. The activation overpotentials (η_{act}) on the cathode (cat) and anode (an) appear as a result of additional potential needed to overcome the barrier imposed by a peak of potential energy before the reactants can be transformed into products at the desired rate [19,27]. Both electrodes have different activation barriers and a logarithmic dependence on the applied current density j [19]. The equation describing the overpotential as a function of the applied current is the concentration-dependent Butler-Volmer equation which is fundamental in electrochemistry [27,28].

$$j = j_0\left(\frac{c_{red}}{c_{red,0}}\exp\left(\frac{\alpha F}{RT}\eta_{act}\right) - \frac{c_{ox}}{c_{ox,0}}\exp\left(\frac{-(1-\alpha)F}{RT}\eta_{act}\right)\right) \quad (5)$$

The term j_0 is the exchange current density and is the magnitude of the equal anodic and cathodic currents at an electrode when there is no net current. Even in this situation, reduction and oxidation reactions occur, and the exchange current density gives their current density [19,27]. The local concentrations c_{red} and c_{ox} of reductant and oxidant at the electrode surface can often be assumed to be equal to their equilibrium or bulk concentrations $c_{red,0}$ and $c_{ox,0}$, respectively. For example, for the cathodic hydrogen evolution reaction (HER), the oxidant water and reductant hydroxide both appear in such large quantities that their variation can be neglected. Note that at the cathode the current density and activation overpotential $\eta_{act,cat}$ are taken to be negative,the absolute value is taken in Equation (4).

The coefficient α (charge transfer coefficient, or symmetry factor) is related to the shape of the activation energy barrier. For a single electron-transfer step it has a value between 0 and 1, although practical effective values may exceed unity [29].

At the anode, Equation (5) can be simplified into Equation (6) (when $\alpha = 0.5$ and $\frac{c_{red}}{c_{red,0}} = \frac{c_{ox}}{c_{ox,0}} = 1$) [30,31]

$$\eta_{act} = b\,\mathrm{asinh}\left(\frac{j}{2j_0}\right) \quad (6)$$

Where the Tafel slope is defined as $b = \frac{RT}{\alpha F}$. Or into the Tafel equation (7) if the applied current density is large [8].

$$\eta_{act} = b\,ln\left(\frac{j}{j_0}\right) + b\,ln\left(\frac{c_{red,0}}{c_{red}}\right) \quad (7)$$

The second term here is the concentration-overpotential due to a reduced concentration of reductants. At the anode, depending on the rate-determining step in the reaction, and in agreement with the reactions in Table 1, the reductant concentration c_{red} can be that of hydroxide ions. Usually, the mass transfer is sufficiently fast so this concentration deviates little from the bulk concentration $c_{red,0}$. At relatively low electrolyte concentrations well below 1 M [32] or in the absence of mixing of anolyte and catholyte [32–34] can this reactant depletion be observed.

Besides the activation overpotential, when current flows through the cell, it will also encounter resistive effects that increase the cell's voltage; thus, an ohmic overpotential (η_{ohm}) will appear. For a layer of electrolyte of thickness l with effective conductivity κ_{eff} Ohm's law and Pouillet's law combine to give $\eta_{ohm} = jl/\kappa_{eff}$. An alkaline water electrolyzer diaphragm can be characterized by a porosity ε, denoting the volume fraction of electrolyte, and tortuosity τ, denoting the average ionic path length over the shortest path length. The conductivity of the electrolyte, which strongly increases with increasing temperature, is decreased because of these effects to give $\kappa_{eff} = \kappa_0\varepsilon/\tau$. For the popular Zirfon-Perl diaphragm $\varepsilon \approx 0.5$ and $\tau \approx 1.5-3$, or even higher if you take into account the additional path-length introduced by zero-gap electrodes and the presence of bubbles [32]. For a PEM electrolyzer, the resistivity of the membrane depends strongly on its water content and temperature [35].

The typical current-voltage (I–V) curve or static characteristic of the electrolyzer is shown in Fig. 3.

The I–V curve can also be reproduced by an empirical model relating the current density (defined as the current, I per unit area, A), of which the model proposed by Ulleberg [37] for an alkaline electrolyzer (Equation (8)) is one of the most widely used because it allows an easy fit to any technology (with the parameters r_x, t_x and s) and include the effect of temperature (T) on the I–V curve.

$$E_{cell} = E_{rev} + \frac{r_1 + r_2T}{A}I + s\,log\left(\frac{t_1 + \frac{t_2}{T} + \frac{t_3}{T^2}}{A}I + 1\right) \quad (8)$$

The thermal model is based on a lumped thermal capacitance C_t as seen in Equations (9)–(11) [37] with Nc the number of cells of the electrolyzer and R_t the thermal resistance of the cell [37].

$$C_t\frac{dT}{dt} = \dot{Q}_{gen} - \dot{Q}_{loss} \quad (9)$$

$$\dot{Q}_{gen} = N_c(E_{cell} - E_{tn})I \quad (10)$$

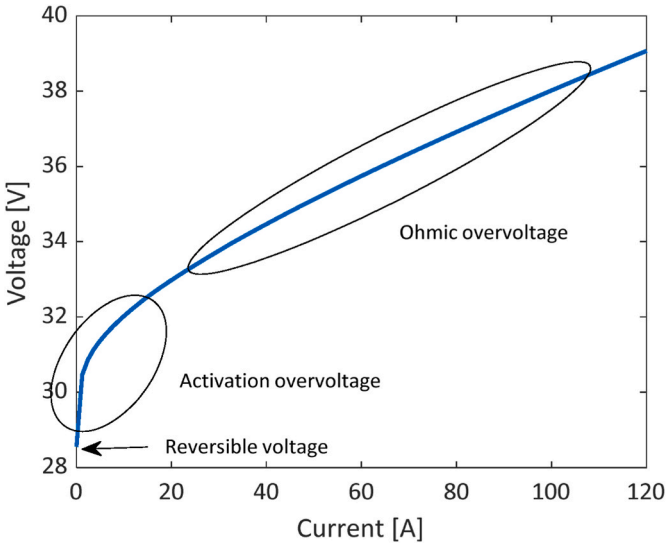

Fig. 3. Example of an I–V curve of a 4.6 kW alkaline electrolyzer. The effects of the overpotentials are shown. I–V curve obtained with data from Ref. [36].

$$\dot{Q}_{\text{loss}} = \frac{1}{R_t}(T - T_{\text{amb}}) \tag{11}$$

3.2. Electrical dynamic response

The voltage evolution occurs in two phases when a current step is applied to a PEM cell. First, an immediate response will set the response along the instantaneous characteristic curve (called "iso-η-line") [38], which is different from the I–V polarization curve. This first response will often lie outside the polarization curve. After this initial response, a dynamic response will move this initial point towards the I–V curve [38,39]. The full path is illustrated in Fig. 4.

The dynamic response is highly non-linear [39,40]. In fact, it can take an 8th order transfer function to accurately reproduce the actual voltage response of a device [40]. With a simplification, three time-constants can be identified. Two of which are extremely fast and resolve in approximately 13 ms and one main time-constant of approximately 1 s [39,40].

The dynamic phase will also depend on [39].

- The direction of the step
- The type of step (voltage, current, or power)
- The magnitude of the step

The initial response of a large downward voltage step can be a negative current. During this negative overshoot, the current is reversed, and its magnitude depends on the ohmic losses. The lower the losses, typically associated with thinner membranes, the higher the current reversal [39]. Similar behavior occurs in AEM cells, but the current reversal and overshoot can reach a considerable magnitude (almost 2 A/cm^2 in both directions) with high voltage steps (2.1 V–0 V) [41].

The electrolyzer dynamics can be represented using an equivalent circuit model that characterizes the behavior of fast-occurring reactions at an electrode. It models the electrical double layer as a capacitor. In parallel, a resistance in series with a second capacitor characterizes the speed of the reaction. The parallel branch is connected in series with a resistor simulating the resistance of the electrolyte. This circuit, called *Randles equivalent circuit* [42], is illustrated in Fig. 5(a). A modified version of the Randles circuit, which is often found in literature, is shown in Fig. 5 (b). Each of the two R–C branches represent one electrode [36,43,44].

The capacitors can be replaced with non-ideal capacitors modeled as Warburg impedances [45,46], to model the losses caused by reactants consumed or products not being quickly removed, or Constant Phase Elements to model the uneven distribution of current in the electrodes [43,45]. The circuit can also be simplified by ignoring the capacitors and introducing controlled voltage sources [36,47–49] or diodes [50–52] to approximate the response of the I–V curve.

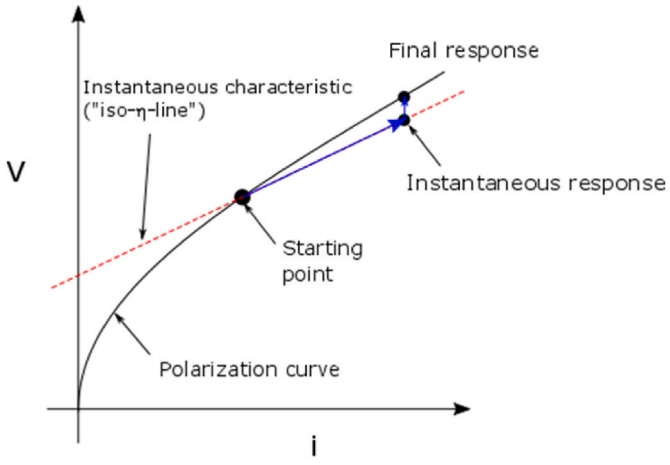

Fig. 4. The path on the I–V plane after a step response. The instantaneous characteristic marks all the possible points where the immediate response can occur from the current starting point. Adapted from Ref. [39].

The electrical response of an electrolyzer can be explained using Figs. 4 and 5(b). Suppose that the electrolyzer is operating at the point marked as "starting point" in Fig. 4 at steady state, so there is no current flowing through the capacitors of Fig. 5(b). Upon applying a current step, the current will flow immediately through the resistors of Fig. 5(b) causing an instantaneous increase in the electrolyzer's voltage leading to the point marked as "instantaneous response" of Fig. 4. The capacitors will begin charging causing the drift of the operating point towards the point marked as "Final response" in Fig. 4 [38].

As the initial response of the cell is exceptionally rapid, its voltage response can be approximated as a first-order system [32,47]. The voltage response of a 12.25 cm^2 PEM cell (H-TEC Energy Systems) to a current step followed the exponential approximation typical of first-order systems [47]. The steady-state was reached in approximately 4 s. For an alkaline cell, the behavior exhibits a similar trend. The voltage response *E(t)* of an electrolyzer cell is an exponential function of the form (12) [44]:

$$E(t) = (E_0 - E_\infty)exp\left(-\frac{t}{\tau}\right) + E_\infty \tag{12}$$

The terms E_0 and E_∞ represent the starting and steady-state voltage, respectively.

For alkaline cells, the first-order behavior can be attributed to bubbles. While describing the effect of bubbles under a zero-gap configuration, Haverkort and Rajaei [32] found a response time of approximately $\tau \approx 10$ s, whose behavior is also characterized by an exponential (Equation (12)). This is associated with the build-up of an additional resistance tentatively attributed to the formation of bubbles. After introducing a small gap between the electrode and the separator, the additional resistance and associated voltage appearing over the mentioned response time, disappeared.

Faster dynamics remains, related to the capacitance of electric double layer (EDL). The supporting information of [32] shows for a single small alkaline cell an associated time-scale of around 1 min at a very low current density of 1 mA/cm^2; decreasing to a fraction of a second for higher current densities [33].

A longer time scale can be associated with diffusion processes. In a porous diaphragm, without any flow through it, half of the current can be transported by diffusion in steady-state. But for steady-state concentration profiles to develop it takes a time of the order of $l^2/4D_a$, with l the diaphragm thickness and D_a the effective medium ambipolar salt diffusion coefficient [33].

Even longer time-scales are associated with changes in the electrolyte concentration. Operation at a significant fraction of the limiting current density gives rise to concentration differences between anolyte and catholyte. When these are not re-combined effectively, depletion of hydroxide at the anode may over time cause an increase in concentration and ohmic overpotential [32–34]. In the absence of flows, the time-scale associated with this is $lV/4AD_a$, with V the combined anolyte and catholyte volume and A the electrode area. For the small single cell studied in Ref. [33] this time-scale was of the order of an hour, but it can be substantially more, including the volume of the piping, manifolds and gas-liquid separators. On a time frame ranging from hours to months, the voltage of an electrolysis cell starts to rise considerably. This voltage rise begins approximately 30 min after the start-up and might continue for months. The cause is attributed to the hydrogen absorption in the electrodes and their oxidation [53].

Moving to a larger scale, the dynamic response of 40 kW PEM and alkaline electrolyzers was studied experimentally in Ref. [54] by applying power steps from 25% to 50%, 75% and 100% (ramp-up) and from 100% to 75%, 50% and 25% (ramp-down) and measuring the electrolyzer's current. The objective was to determine the suitability of

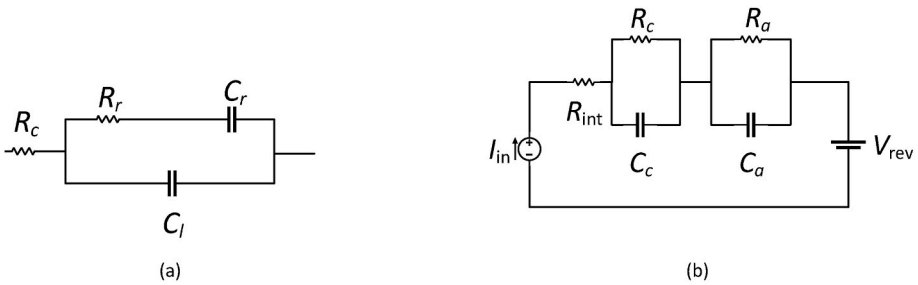

Fig. 5. (a) Randles circuit. R_c represents the resistance of the electrolyte. The electrical double layer is represented by C_l, while R_r and C_r form an equivalent impedance modeling the speed of the reaction. Adapted from Ref. [42]. (b) Equivalent circuit with two RC networks, one for each electrode. R_{int} represents the ohmic losses and V_{rev} the reversible voltage. Adapted from Ref. [44]. These circuits can be applied to PEM, AEM or AEL.

both technologies to operate under these conditions. Part of the experiment consisted of quantifying the initial response time when the electrolyzer needs to start responding and reach 1% of the maximum current after a change in the set-point. For the measured electrolyzers, it was determined to be 13 ms and 19 ms for PEMEL (Proton OnSite, 40 kW, three stacks) and AEL (Teledyne Technologies, 40 kW, 75 cells, one stack), respectively. This value is influenced by other components such as power electronics of the power supply that also need time to react [54]. Both electrolyzers required less than 0.2 s to reach more than 90% of the final current value (*settling time*). The settling time is influenced by the step size and the direction of the ramp. A more significant step will result in a slower response [54]. The authors report that the measurements were taken only for 0.2 s due to equipment limitations.

The ramp rate was also calculated as the ratio of the percentage of the maximum current per second. PEMEL have slightly higher ramp rates than alkaline electrolyzers, meaning that they can reach the maximum current in less time [54].

3.3. Influence of temperature and pressure

Temperature has an impact on the electrolyzer's voltage. As temperature increases, the activation overvoltages tend to be higher as the Tafel slope is also higher (see Equation (7)). However, for low overvoltages, temperature also causes a rise in the exchange current density j_0 which, in turn, reduces the activation losses [27]. Higher temperature also results in lower resistive losses [21,55,56] as well as lower reversible voltage [10] (see Sections 2 and 3.1). The benefits of lower ohmic losses overcome the negative influence of temperature [27]. For this reason, temperature is considered to impact the electrolyzer's voltage positively [21]. This influence on the electrolyzer's voltage affects the electrolyzer's efficiency. At lower temperatures, the demanded power to produce hydrogen is higher [57] (lower efficiency).

Temperature also influences the operating voltage and the gas purity (HTO - Hydrogen-To-Oxygen) [55] as the diffusivity and solubility of the produced gases depend on temperature. Sanchez, et al. [55] found that the HTO content increased around 4% with only a 5% temperature increment.

On the other hand, pressure has a minor effect on the polarization curve of alkaline electrolyzers than that of temperature. Even a deviation of 10% from the pressure reference results in a negligible effect on the voltage [55]. This is not the case for the gas cross-over. A pressure difference between the cathode and the anode further enhances the convective transport of gas through the separator. Since the permeability of Zirfon™ (commonly used for separators in alkaline electrolyzers) is higher than Nafion™ (the most used membrane material for PEM), AELs are more susceptible to pressure gradients between cathode and anode. Even when operating at equal pressures in AELs, the control valves can create a slight pressure gradient contributing to gas cross-over [58]. In fact, the HTO can rise by 2% with a pressure increment of 10% [55].

The performance of AEM with pressure is worse than PEM but better than AEL [59]. It lowers the Faraday efficiency and has a minor effect on the ion conductivity of the membrane. This causes a slight increase in its resistance, with a consequent increase in the cell's voltage which is limited to 11 mV when the applied current is 1 A/cm^2 [59]. The pressurized operation, like PEM and AEL, impacts the gas crossover. The hydrogen permeation flux from cathode to anode increases linearly with pressure, and the HTO reached dangerous levels at low currents (0.1 A/cm^2) and high pressure (8.5 bar) [59].

Temperature and pressure influence the operating conditions of electrolyzers. According to Ogumerem and Pistikopoulos [60], the dynamic behavior of the electrolyzer is dominated by the temperature. While developing a control strategy for a simulated PEMEL, the voltage immediately follows the step after a current change but then decays slowly as the temperature increases. Colbertado, et al. [61] reached a similar conclusion for a 12-cell, 160 cm^2, simulated PEMEL, although their observations did not include the voltage evolution in time, only the temperature. In terms of power consumption, stepping down from a higher power and temperature setting to a lower power is more beneficial than the opposite [57]. This does not mean that the electrolyzer cannot shift to the new power point, but the efficiency (which is temperature dependent and higher at higher temperatures) will be reduced as the temperature rises to the new set point [57].

Pressurized operation improves the ramp rate of alkaline electrolyzers. The ramp rate is limited to keep the gas volume inside the cells always within controllable limits by ensuring that the gases are adequately vented. High pressure facilitates the expulsion of gases leading to higher ramp rates than atmospheric-pressure operation [62]. However, this benefit can only be achieved once the pressure set-point has been reached. During a cold-start, the leading cause of delay is pressure build-up. Additionally, if the electrolyzer goes into standby mode, the pressure needs to be maintained [62].

The gas cross-over increment with temperature and pressure can have severe consequences as the lower explosive limits (3.8% mol H_2 at 80 °C and 1 atm for a 15 kW alkaline electrolyzer) can be exceeded [55].

4. Operating under varying conditions

There are two ways of starting the operation of an electrolyzer. Suppose the electrolyzer is off, cold, and depressurized (for example, at the beginning of a day or after a long period when it is not being used). In that case, the system needs to be warmed up before it can start producing hydrogen. This is called a cold-start. Another situation is a short interruption where pressure and temperature and pressure can be maintained, and the production can continue without delays. This is a warm-start [54].

The steps that are needed during the cold-start are illustrated in Table 2.

The first consequence of variable power is that this process is interrupted if the system cannot reach the minimum operating pressure within a specific time range after start-up. This is illustrated with a Proton OnSite HOGEN RE40, PEM electrolyzer. This unit will interrupt

Table 2
Cold-start sequence. The times for the PEM electrolyzer are based on a Proton OnSite C10, 60 kW nominal power [63]. The alkaline electrolyzer times are reported for a 24 kW pressurized (12 bar) unit [62]. Step 2, involves removing the air in the piping system [63] or, in the case of the alkaline unit, injecting nitrogen to remove residual hydrogen in them [62]. The AEL electrolyzer data is published by ENAPTER [64]. The ramping up time for all technologies includes the necessary time to build up the hydrogen pressure.

Step	Process	PEM [63]	Alkaline [62]	AEM [64]
1	Booting the control unit	0.5 min	N/D	N/D
2	Purging pipes	2–10 min	25 min	N/D
3	Ramping up to full power	3 min	10 min	25 min

the process if the operating pressure of 14 bar is not reached within 30 s [65]. In order to prevent this, a minimum operating load is set (34% of nominal power for the previous example [65]). This minimum load is well above the minimum load required when operating under normal conditions (7.6% of nominal power for PEM [65], 18% for alkaline [62], and up to 60% for AEM technology [64]). As a result, due to the minimum load requirement along with the relatively long time that is needed for a cold-start, the maximum number of times the system can be stopped and restarted in a day is limited [62,64].

The ramping rate indicates how fast can the electrolyzer react upon a change in power. The PEM technology has power ramps in the range of 10%/s [66] (change in power of 10% of the current operating set point) to +50%/s and −40%/s [67]. [63]Alkaline technology has ramp rates of 0.3%/s [68], 2.5 kW/s or 308 kW/s [62]. For AEM the ramping up rate is +0.47%/s (ramping up) and a faster ramping down rate up to −10%/s [64]. In general, electrolyzers can react faster to down-ramps than up-ramps. Based on the discussion of Section 3, and the observations of [62], the slowest variables (pressure, gas venting, temperature) along with the control system impose the limits on the ramp rate, rather than the electrical capability of the stack to manage the power changes. Limiting the ramping of the electrolyzer has little effect on the levelized energy cost, as long as these are constrained to a minimum of 15% of the rated power. If the ramps are restricted to shallower levels, the impact on the cost becomes significant [69].

For a PV system, the ramping rate is between +0.098%/s and −0.078%/s [68] which is slower than the rate at which electrolyzers can respond. Note that the ramping values were originally reported per minute and converted to per second for consistency. However, measured ramps in the per second scale can reach considerable higher values, which are not reflected in a per minute analysis. In this respect, PEM has proven to be able also extreme ramping events managing to respond upon +80% and −100% change in power within 1 s [63]. The fast reaction times of large-scale electrolyzers make them very attractive for grid frequency support and can play a role in future energy systems, marked by the absence of rotational inertia [67,70]. In fact, the two main low-temperature technologies, AEL and PEM have received approval for their use as ultra-fast ancilliary services [17].

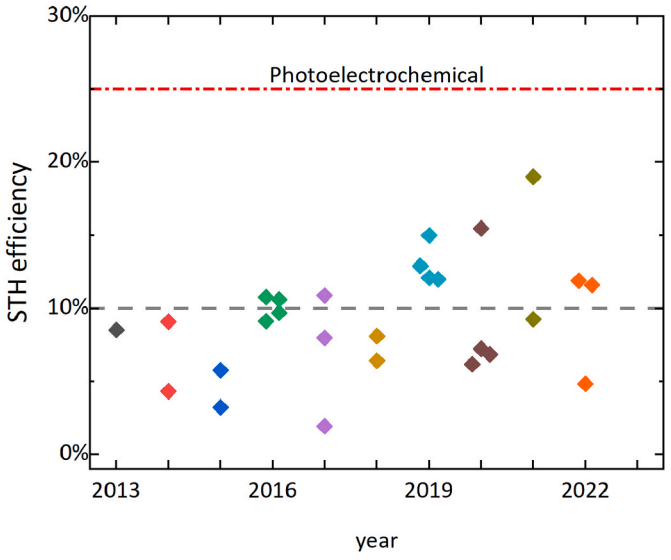

Fig. 7. Solar-To-Hydrogen efficiency per year as reported in literature [65, 72–80,82–89,90–95]. The dashed line marks the limit above which the STH becomes economically feasible [96]. The dashed-dot line with the legend "Photoelectrochemical" indicates the target of the Department of Energy of the USA for a photoelectrochemical devices [97]. Although it is a different technology than the one addressed in this work, it provides a point of comparison as there is no specific target for the STH of a PV-hydrogen system.

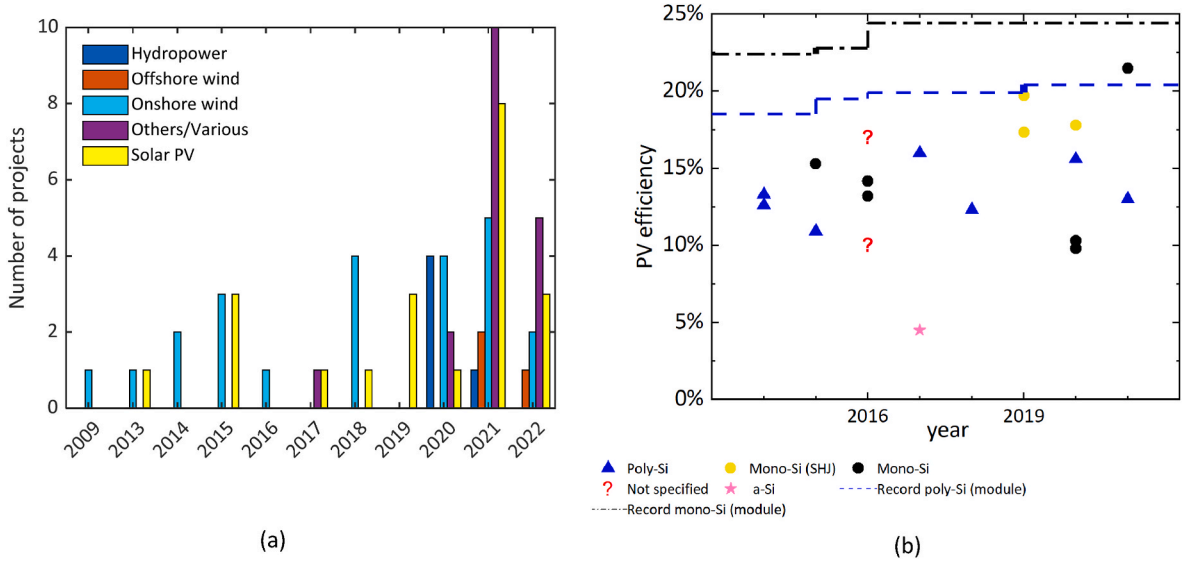

Fig. 6. Renewable technologies used to drive large-scale electrolysis projects for hydrogen production worldwide. With data from Ref. [6]. (b) Efficiency of the PV module reported in literature classified per technology [65,72–89]. The dashed and dash-dot lines indicates the record efficiency for a poly-si and mono-si module, respectively [71].

4.1. Coupling with solar energy

PV energy is becoming an attractive option for powering electrolyzers. This can be seen in Fig. 6(a). While at first, onshore wind was the preferred technology, in the last years PV is becoming the preferred technology. It does not need to substitute wind power, but can also coexist (Fig. 6(a), group "Others/Various"). Fig. 6(b) shows the efficiency of solar modules used in literature during the past 10 years, as well as the record efficiency for modules with different cell technology [71] .

To evaluate a solar-powered hydrogen project, the Solar-To-Hydrogen efficiency is introduced. It is defined as the ratio of the generated hydrogen to the needed irradiance to produce such amount (Equation (13)) [98].

$$\mathrm{STH} = \frac{\dot{h}_2 \times \Delta G}{S \times A} \tag{13}$$

The numerator term converts the flow of hydrogen ($\dot{h}_2$ in mol/s) into energy. The denominator indicates the amount of irradiance (S, in W/m^2) that the module area (A, in m^2) receives. The STH is a non-dimensional number relating hydrogen energy and solar energy.

Fig. 7 shows the evolution of the STH reported in the reviewed literature over the last ten years.

The coupling factor (or coupling efficiency) defines the ratio of the PV module used relating the operating power ($P_{pv} = I_{pv} \times V_{pv}$) against the maximum power (P_{mpp}) of the module at a particular instant (Equation (14)) [99]

$$\mathrm{CF} = \frac{I_{pv} \times V_{pv}}{P_{mpp}} \tag{14}$$

The coupling factor is also an non-dimensional number with values ranging between zero (no coupling) to one (operating power is at the maximum power point of the module) [99].

4.1.1. Direct-coupling systems

The simplest way to integrate a PV system with an electrolyzer is to connect the PV array directly to the electrolyzer. This is possible as both devices work with direct current. Fig. 8(a) shows a schematic of this configuration. In the directly coupled systems, the operating point is right at the intersection of the I–V curves of the PV array and the electrolyzer, as seen in Fig. 8(b). In practice, the system operates away from the MPP of the PV because the polarization curve of the two devices is not well matched. These systems need to be optimized in such a way that the I–V curves of both components are close to the MPP of the PV module. This optimization can be based on setting the MPP of the PV close to the region of operation of the electrolyzer with higher probability of occurrence [100]. Then, the number of series-connected electrolyzer cells, as well as the configuration series-parallel of the solar cells, both curves can get closer to the MPP [93,100].

Direct-coupling systems have minimum control capabilities, limited to a simple ON-OFF control in case of the electrolyzer operating below the safety threshold or exceeding its nominal capacity [74,101]. However, the directly coupled system can be optimized by dynamically changing the connection of the electrolyzer cells. Using an external contactor or switch, the number of electrolyzer cells can be incremented or reduced. This adds another level of control, facilitating the matching of the electrolyzer to the MPP of the PV module. This operating strategy is essentially a "discrete MPPT" which increases the coupling factor (14) [76,102].

In general, directly-coupled systems have lower efficiency that their DC-DC-coupled counterparts [74,102,103]. The directly-coupled system can boost its coupling efficiency up to 99% if the discrete MPPT strategy described above is used [102].

4.1.2. Coupling with electronic converter

The PV and electrolyzer can be decoupled so each component operates at different regions of their I–V curve. In this way, the PV modules can operate at maximum power point with the consequence that the electrolyzer will also operate at this maximum power, limited only by the efficiency of the converter [92]. Note that the efficiency of the converter is different from the coupling efficiency. In these systems, the coupling efficiency is virtually 100% as the converters implement a maximum power point tracker that forces the PV to deliver the maximum power. The electronic converter also has an efficiency of its own (Fig. 10(b)), and it degrades considerably if operated at a lower load than its nominal rating [74]. This efficiency affects the Solar-To-Hydrogen efficiency [103] which can be seen in Fig. 10(a).

Direct coupling systems are best suited in systems where the PV and the electrolysis systems share the same physical location. Indirect coupling (using an electronic converter) allows to cover both scenarios: same physical location or the case where there's a considerable distance between both systems.

In the latter, To transport the electricity from PV to the electrolyzer, either a high-voltage DC transmission system (with the consequence that a series of DC-DC converters are needed (Fig. 9(a))) or a traditional AC system (with the need of at least one DC-AC conversion stage, a transformer and finally an AC-DC rectifying stage at the electrolyzer side Fig. 9(b)) [102].

When DC/DC is used, many converter topologies can be used, which are extensively reviewed in the work of Guilbert, et al. [105]. In particular, because the voltage of the electrolyzer is smaller than the PV, the traditional buck converter (step-down) converter is an attractive option. Although it suffers from limited conversion range. If the voltage to be stepped-down is considerable, this converter might not work well. Then, an adaptation is needed, which can be achieved by a so-called Quadratic Buck Converter, whose voltage output varies with the *square* of the duty cycle (instead of linearly as the traditional buck). An additional point is reliability in case of a switch failure. Multi switch configurations, such as the interleaved converters allow for a more reliable operation, Although still have the same operating range limitation as the traditional buck [105].

4.1.3. Battery-assisted electrolysis

Because of the variable and intermittent nature of solar-powered electrolysis, the electrolyzer cannot operate at full capacity for 24 h a day without any backup electric storage or support from the electricity

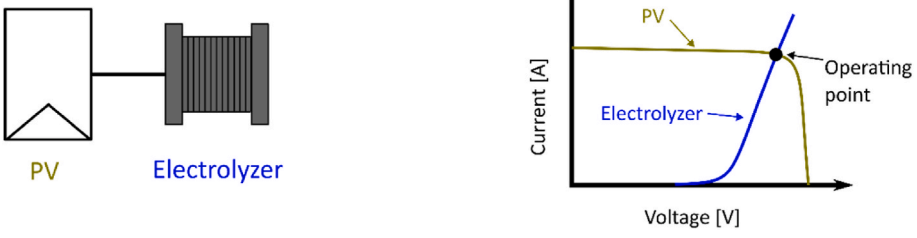

Fig. 8. Direct coupling of PV and electrolyzer (a). The operating point is the intersection of the I–V curves of the two components (b).

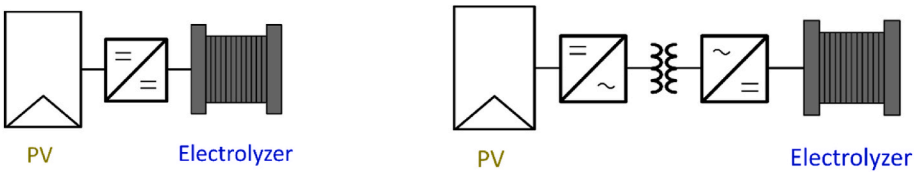

Fig. 9. Coupling PV with electrolyzer using power converters. (a) Coupling using DC-DC conversion. Depending on the system, more than one DC-DC converted might be present [102], and (b), coupling using DC-AC-DC conversion. This configuration needs a transformer to accommodate for different voltage levels [101,102].

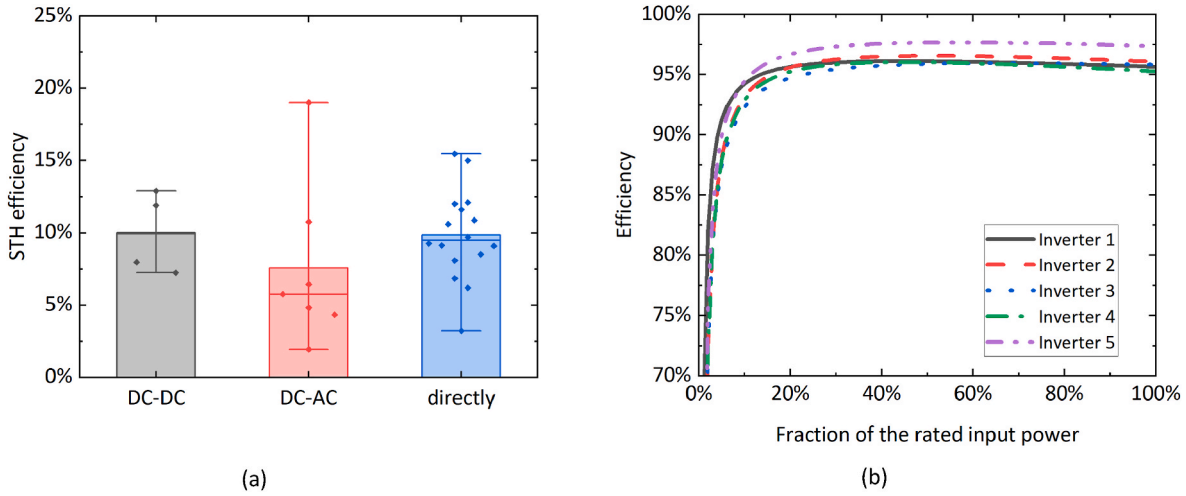

Fig. 10. (a) Comparison of the STH obtained with different coupling types as reported in literature [65,72–80,82–89,90–95]. Note that battery-assisted systems always use an electronic converter. (b) Five random examples taken from the library of the System Advisor Model [104] showing the efficiency at different operating loads of commercially available inverters for PV applications.

grid. Batteries have the potential to smooth the fluctuations in hydrogen production and enhancing the operating time of an off-grid PV-powered electrolyzer.

There are three main operating methods for the PV-battery-electrolyzer system:

1. The battery supports the electrolyzer in periods where PV is not enough to start the electrolysis process by supplying enough power to operate the electrolyzer at its technical minimum [87,89,106].
2. The electrolyzer is operated at a fixed power, which is lower than its nameplate capacity. The battery provides or stores energy as needed to keep the constant operating point of the electrolyzer [89].
3. The electrolyzer operates at a constant set point, which changes daily or seasonally [89,106,107].

Whether adding batteries to the electrolysis system is economically feasible or not it is still a matter of discussion. Hybrid systems combining PV and wind or simply curtailing a fraction of the PV production lead to cheaper hydrogen prices and acceptable payback times of 15 years with a hydrogen cost of 4 €/kg, or only 5 years if the cost increases to 7 €/kg [108]. Grid-connected systems without battery support also have lower hydrogen costs (4.22 €/kg) than their off-grid counterparts (around 6 €/kg) [89].

On the other hand, batteries can significantly reduce the size of the components. Koyama [109] argues that with the battery-assisted system, the electrolyzer unit is small, resulting in a reduced amount of investment costs. The savings from the electrolyzer investments are compensated by the installation costs of the battery which can account up to 33.6% of the hydrogen cost [89]. The battery has the potential to increase the amount of hydrogen produced during intermittent periods (such as the day-night cycle) [107]. The hydrogen production can be boosted more than 100% (utilization factor) by adding batteries and has the potential to outperform a PV-wind hybrid system without them by 2.4% [76,107,108].

The environmental impact of battery-assisted electrolysis is mainly driven by the production of PV modules and batteries and considerably lower, in terms of greenhouse emissions than the fossil-fuel based processes. But the need for non-renewable, non-living resources (Abiotic Resource Depletion) results in higher impact that fossil fuel methods. This only points out that other challenges need to be solved besides component sizing and cost reduction [110].

4.2. *Consequences of variable operation*

Changes in solar irradiance or wind speed do not occur instantaneously as in a step but continuously over time (ramp). As these renewable sources are used to power electrolyzers, Lee, et al. [111] determined the effect of current ramp direction and depth on the electrolyzer's efficiency. The efficiency loss is due to the accumulation of gas in the Porous Transport Layers (PTL) that prevents the reactants from reaching the electrodes. The buildup of gas is linked to the current ramps applied to the electrolyzer and depends on the direction of the ramp and its slope. During the ramping process, the gas saturation in the PTL changes linearly, and when the current is kept constant, it changes in a logarithmic way. The gas saturation occurs faster with steep up-ramps, and shallow down-ramps enhance gas removal. Hence, the combination of these two scenarios leads to an improved operation related to the gas response. Further, gas accumulation occurs faster than gas removal. This causes that when the same current is applied twice after a variable operation, the cell voltage will be higher at the second point leading to a lower efficiency [111].

The operating constraints imposed on the electrolysis system will depend on the electrolyzer technology (AEL, PEM or AEM.) Alkaline electrolyzers typically have a partial load operating limit of around 20% of their nominal capacity, while PEMELs offer greater flexibility working at partial loads of 5% of nominal capacity [54,112]. This allows PEMELs

to utilize more energy coming from renewable sources. PEM technology is sometimes argued to benefit from faster ramp speeds. In Ref. [112], the authors considered 10% of nominal power per second for a PEM electrolyzer model, in contrast to 1.67% nominal power per second for their model of an alkaline electrolyzer. These differences do not amount to a significant advantage over the alkaline one in hydrogen production. During periods with low irradiance, the PEM will operate at a low partial load while the alkaline remains off. This additional operating time is not significant in terms of produced hydrogen [112].

At partial load (operation below nominal conditions), the content of hydrogen in oxygen can reach dangerous levels. This is because the hydrogen dissolved in the water or electrolyte is transported to the anode chamber, where oxygen is being evolved. The transport mechanisms are [58].

- Diffusion, as a result of a concentration gradient.
- Convection due to pressure gradients, dissolved gas transport with the ions through the membrane or separator (electro-osmotic drag), and operational strategies (electrolyte mixing, in AEL).
- Supersaturation before the produced gases in dissolved form develop into bubbles.

Gas cross-over increases with pressure and current density; nevertheless, the gas impurity is reduced at higher current densities as the gas production is greater than the permeated gas, so the fraction of the latter in the former is also lower [58].

Mitigation techniques for dealing with the minimum operating power of alkaline electrolyzers include backup electrical storage or using separate units operating in a modular way. Turning off some modules could result in the remaining ones working a higher current densities [113]. Operation strategies can also help reduce gas cross-over and impurities, especially in alkaline technology. Most of the gas cross-over in alkaline electrolysis occurs because the electrolyte from the cathode and the anode is combined in the separator tanks and then recirculated. This electrolyte can be contaminated with gas remains. Hence, using different separator tanks for catholyte and anolyte reduces the gas cross-over, as well as minimizing the recirculation rate. For large electrolysis plants, a constant recirculation rate provides the best strategy [58].

Knowing the time constant of the system can be beneficial in developing operation strategies aiming at improving energy efficiency. The ripple on top of the DC signal causes losses in efficiency [114,115]. But, if the current is interrupted only for short periods, the effect can be the opposite. Interrupting the current for the duration of the time constant (around 2 ms) reduces the polarization overpotential and helps to keep a constant concentration throughout the electrolyte. Removing the current for short periods also facilitates the expulsion of bubbles, potentially decreasing the resistive losses caused by coverage of the electrodes with bubbles [116].

The electrical response reaches a new set-point in a matter of seconds, but it experiences a slow change caused by temperature affecting the ohmic and activation losses. Energy consumption is higher during the temperature transient leading to an efficiency loss of around 5% [117]. Allidières et al. [117] show that the power density reaches the new set point so fast that the temperature of the stack lags. Energy is lost when the temperature rises again to the corresponding operating point. This results from a sub-optimal operating point, as discussed in Section 3.3. Their system consists of a 20-cell PEM stack (the size or the power are not specified) with uncontrolled temperature.

The successful deployment of electrolysis plants depends not only on the stack but also on the auxiliary components (Balance-of-Plant) as highlighted by Furfari and Clerici [118]. Even the International Renewable Energy Agency (IRENA) reports that a hydrogen plant designed for variable operation imposes more constraints on the Balance-of-Plant elements than the stack. The configuration of the latter can help in such operation by using smaller units connected in a modular way [17].

The control of the whole plant also relies on the understanding of dynamic response. Although, this work does not aim to discuss the available operation strategies, it was found in at least two works [119,120] that the misunderstanding of dynamic behavior (at quick and slower scales) can lead to a control system that cannot follow accurately the imposed set-points making the plants unable to follow quick variations imposed by quick changes in renewable power. Other authors have mentioned that ignoring the dynamics of the electrolyzer can lead to considerable efficiency loss [121].

Bifacial modules are an attractive option for boosting hydrogen production of directly coupled PEM electrolyzer systems. Recent experiments show that using a bifacial system, the STH efficiency rises 13% with respect to the monofacial system. This number can be even improved by using materials that boost the reflectivity of the ground [88].

4.3. Potential impacts of intermittency on lifetime

The estimated lifetime of electrolyzers is a critical issue, especially when operating under variable conditions. For alkaline technology, the lifetime of the stack, based on acceptable efficiency drops, lies between 60 000 and 90 000 h, while for PEM this is lower: 20 000 to 60 000 h [122].

The degradation mechanisms that lead to cell failure are listed in the reviews of [123] (for PEM fuel cells) and [124] (for PEM electrolyzer cells).

A higher voltage or a higher current can be detrimental to the electrolyzer. While high voltages accelerate corrosion, the performance loss is minimal compared to using a high current density [125].

The intermittent operation can result in lifetime benefits. For example, 90 000 h can be translated into 20 years of operation if this is intermittent [122] (considering that 90 000 h are roughly 10 years).

On the other hand, intermittency can also represent a challenge as it can accelerate some degrading mechanisms. For instance, Weiβ et al. [126] determined the effect of idle operation where the voltage of the electrolyzer is equal to the open-circuit voltage. They observed an initial improvement of the cell performance after resting periods, where the cell was left at open circuit (10 cycles) followed by performance decrease observed as a higher cell voltage. Mainly, the degradation was related to increased high-frequency resistance due to oxide formed during the open-circuit period. After 700 cycles the high-frequency resistance increased 1.6 times. To overcome this, a voltage of 1.3 V was applied.

When the PEM electrolyzer is switched off, it operates for a short period in reverse mode (i.e., as a fuel cell), consuming the hydrogen and oxygen in the stack immediately after electrolysis is interrupted [127]. During this process, platinum in the cathode electrocatalytic layer is lost as it is transported to the membrane, thus reducing its conductivity [127]. Further, the cathode voltage increases when the electrolyzer is shut down. This voltage increase damages the catalyst causing a reduction of the available area suitable for the reaction [128].

The reverse mode is not a specific characteristic of PEM electrolyzers. As explained by Uchino et al. [129] also alkaline electrolyzers present this behavior when the current is cut. Under this scenario, the dissolved hydrogen and oxygen produced during electrolysis react with the nickel oxide formed at the anode. The reverse current can flow for as long as 100 min.

In AEM, small portions of the catalyst detach from the anode with steep voltage steps. These steps, as with PEM, cause a transitory current reversal, whose magnitude can be considerable (between −100 and −200 mA/cm^2. To put this in context, the cell operated at a maximum current density of 672 mA/cm^2). When the cell is left idle, under open-circuit condition, the membrane becomes dehydrated, leading to increased resistance; hence, even in stand-by conditions, a water flow should be maintained to avoid this situation [41,130].

Rakousky et al. [125] also investigated the degradation caused by the intermittent operation. To determine that effect, they created a reference test operated at constant current at both high and low current densities. For the dynamic operation, they applied steps between three current density levels: 0 A/cm^2 to 2 A/cm^2 (high current density) and 1 A/cm^2 (low current density) to 2 A/cm^2. Different intervals of on-off were also used. The cell is stable, with no degradation when operated at 1 A/cm^2 continuously. At higher current densities, the lowest degradation rates (16 μV/h) were obtained by operating continuously for 6 h followed by a resting period with no current flowing, for another 6 h. However, more frequent shut-downs lead to a worst degradation rate (50 μV/h). These degradation rate are lower than operating continuously at high current density, which leads to the highest degradation rate of 194 μV/h. High current densities lead to electrode damage, especially passivating the anode [125,128]. Also, mechanical damage due to bubbles, possible transport of contaminants as more water is consumed [125] and potential damage to the membrane either by forming hotspots [125] or thinning [128]. This last statement is significant as the loss of membrane material has been found to affect industrial-scale electrolyzers with more than 20 000 h of operation. The thinning was attributed to material loss due to a chemical interaction rather than a mechanical process associated with bubbles [131]. Nevertheless, the thinning of the membrane can also be attributed to high temperatures, which can drastically increase the thinning process [132]. Furthermore, the membrane can suffer from puncturing, associated with hotspots appearing. This can destroy the stack because of a dangerous mixture of hydrogen and oxygen in the chambers [133].

Nonetheless, the degradation attributed to intermittency is not entirely clear from an electrochemical point of view. Some studies have found that continuous operation exhibits the same degradation that dynamic operation, so the aging mechanisms cannot be attributed to a highly dynamic process [134]. Degradation might be linked to mechanical stress caused by temperature and pressure variations, and the operation with renewable energy does not necessarily accelerate the aging process [11].

5. Conclusion and discussion

This review presented the integration of electrolyzers with PV systems aiming at green hydrogen production focusing on the three main low-temperature water electrolysis technologies implemented nowadays: alkaline, Proton Exchange Membrane and Anion Exchange Membrane. Water electrolyzers are well suited for integration with variable renewable power as proven by this review and supported by other studies and international certifications. The electrical dynamic response has a minor influence on the electrolysis system and is related to the implementation of control systems. Slower dynamics introduced by temperature and pressure play a more important role in their integration with solar energy. The limitations for the electrolyzers when operating in variable mode, are mainly due to the operating limits of the electrolyzers, especially regarding the minimum operating limit required for safety operation. There is no clear evidence of degradation with a variable operation. Rather, the degradation effects can be caused by improper operation: higher current densities, frequency shut-off and keeping the stack at open-circuit voltage. In this respect, *intermittency* rather than *variability* of the power source play a more relevant role in limiting the integration of electrolyzers with renewable energy.

When powered from PV systems, the solar-to-hydrogen efficiency needs to exceed 10% for a system to be economically feasible. In the last 10 years there have been improvements towards this objective, yet there are still recent studies that fail to meet this goal. One of the potential causes for this is the definition of efficiency itself. Different authors use different definitions from it, ranging from: *solar-to-hydrogen efficiency*, *MPPT efficiency, Faraday's efficiency* and *energy efficiency*. The latter is also often calculated with either the low or the High Heating value of hydrogen leading to different results. This indicates a lack of standardization and direction on the research lines. This is even marked by the absence of a tangible goal for STH efficiency for PV-hydrogen systems. The goal reported in this work of 25% represent the target of a photoelectrochemical device, but not for PV powered systems. Even if it were the case, the development of PV-hydrogen systems is still very far from this target. Stand-alone systems without storage represent the area where there are more efficiency improvements needed. The coupling efficiency can reach impressive high values close to 99%. In this respect, the improvements in efficiency are linked to the efficiency of the electrolyzer, which is improved by using PEM technology, and the PV system itself. In spite of the advances in the efficiency of PV modules, this still has not fully reached the enough maturity, or cost reduction to be practically implemented. Further, we found only one work discussing bifacial PV systems which could improve the overall PV system efficiency, hence the STH. Research opportunities include focusing on more innovative PV applications besides the typical rack-mounted panels: bifacial PV, agrivoltaics, floating PV, etc. provide new opportunities to explore their integration with hydrogen systems.

Another challenge associated with the variable operation of PV-hydrogen systems is the availability of high-resolution data. Hourly data cannot properly capture the variability of the irradiance, and is only suitable for steady-state analysis. However, for variable operation of electrolyzers, their operation can change in seconds while temperature changes in minutes. Sub-hourly datasets or measurement equipment are better suited for variable operation studies. And with the partial load operation of electrolyzers and converters, the assumption of a constant efficiency of either of them can lead to an overestimation of the produced hydrogen. Simple models that calculate the efficiency as a function of the input power, which are also computationally cheap might help in the simulations of PV-hydrogen systems. Since many works are concerned with optimization, where a complex dynamic model might considerable increase the computation time, the assumption of a constant electrolyzer, or Faraday efficiency becomes attractive.

Battery-assisted electrolysis provides a solution to solar energy intermittency. The drawbacks for this technology is the cost, which is the topic of current research and the environmental issues associated with batteries. For projects in the MW range grid-connected systems are typically considered, which facilitates the continuous operation of the plant and reliable production of hydrogen. For smaller projects, such as refuelling stations, DC-DC systems or even directly coupled systems are well-suited.

With this review the challenges of integration of electrolyzers with solar energy can be identified and tackled, helping to achieve the goals set by international organisations and reaching a net zero emission future.

Declaration of competing interest

The authors declare that they have no known competing financial interests or personal relationships that could have appeared to influence the work reported in this paper.

Data availability

The database used in this review is publicly available from the International Energy Agency

Acknowledgements

This activity is co-financed by Shell and a PPP-allowance from Top Consortia for Knowledge and Innovation (TKI's) of the Dutch Ministry of Economic Affairs and Climate in the context of the TU Delft e-Refinery program.

References

[1] International Energy Agency. Net zero by 2050. 2021. Paris.
[2] National Academy of Engineering, National Research C, Division on E, Physical S, Board on E, Environmental S, et al. The hydrogen economy : opportunities, costs, barriers, and R&d needs. Washington, D.C., UNITED STATES: National Academies Press; 2004.
[3] IEA. The future of hydrogen. IEA; 2019.
[4] Stoker L. Iberdrola unveils plans for 'Europe's largest' solar-storage-hydrogen project. PVTECH; 2020.
[5] Ratcliffe V. Saudi arabia's bold plan to rule the $700 billion hyrogen market. Bloomberg Green; 2021.
[6] IEA., IEA. Hydrogen projects database. IEA; 2021.
[7] Dincer I, Zamfirescu C. Chapter 3 - hydrogen production by electrical energy. In: Dincer I, Zamfirescu C, editors. Sustainable hydrogen production. Elsevier; 2016. p. 99–161.
[8] Pera M-C, Hissel D, Gualous H, Turpin C. Electrochemical components. Somerset, UNITED STATES: Wiley; 2013.
[9] Sankir M, Sankir ND. Hydrogen production technologies. John Wiley & Sons; 2017.
[10] LeRoy RL. The thermodynamics of aqueous water electrolysis. J Electrochem Soc 1980;127:1954.
[11] Godula-Jopek A, Stolten. D. Hydrogen production : by electrolysis. Berlin, GERMANY: John Wiley & Sons; 2015. Incorporated.
[12] Mazloomi SK, Sulaiman N. Influencing factors of water electrolysis electrical efficiency. Renew Sustain Energy Rev 2012;16:4257–63.
[13] Amores E, Rodríguez J, Carreras C. Influence of operation parameters in the modeling of alkaline water electrolyzers for hydrogen production. Int J Hydrogen Energy 2014;39:13063–78.
[14] Nagai N, Takeuchi M, Kimura T, Oka T. Existence of optimum space between electrodes on hydrogen production by water electrolysis. Int J Hydrogen Energy 2003;28:35–41.
[15] Angulo A, van der Linde P, Gardeniers H, Modestino M, Fernández Rivas D. Influence of bubbles on the energy conversion efficiency of electrochemical reactors. Joule 2020;4:555–79.
[16] Santoro C, Lavacchi A, Mustarelli P, Di Noto V, Elbaz L, Dekel DR, et al. What is next in anion-exchange membrane water electrolyzers? Bottlenecks, benefits, and future. ChemSusChem 2022;15.
[17] IRENA. Green hydrogen cost reduction: scaling up electrolysers to meet the 1.5°C climate goal. Abu Dhabi: International Renewable Energy Agency; 2020.
[18] Warshay Marvin, Prokpius PR. The fuel cell in space: yesterday, today and tomorrow. 1989.
[19] Solar hydrogen generation : toward a renewable energy future. New York, NY: Springer; 2008.
[20] Sutton A. Nafion: properties, structure and applications. Hauppauge, UNITED STATES: Nova Science Publishers; 2016. Incorporated.
[21] Selamet OF, Acar MC, Mat MD, Kaplan Y. Effects of operating parameters on the performance of a high-pressure proton exchange membrane electrolyzer. Int J Energy Res 2013;37:457–67.
[22] Li C, Baek JB. The promise of hydrogen production from alkaline anion exchange membrane electrolyzers. Nano Energy 2021;87.
[23] Miller HA, Bouzek K, Hnat J, Loos S, Bernäcker CI, Weißgärber T, et al. Green hydrogen from anion exchange membrane water electrolysis: a review of recent developments in critical materials and operating conditions. Sustain Energy Fuels 2020;4:2114–33.
[24] HydroLite. https://www.hydrolite-h2.com/aem-electrolyzer-technology/.
[25] Enapter. https://www.enapter.com/.
[26] Keow ALJ, Chen Z. Auto-tuning control of proton exchange membrane water electrolyzer with self-assessment and gain scheduling. J Dynamic Syst, Measurem Control, Transact ASME 2021:143.
[27] O'Hayre R, Cha S-W, Colella WG, Prinz FB. Fuel cell fundamentals. third ed. John Wiley & Sons; 2016.
[28] Allen J, Bard LRF. Electrochemical methods. Fundamentals and applications. second ed. John Wiley & Sons; 2001.
[29] Parsons R. General equations for the kinetics of electrode processes. Trans Faraday Soc 1951;47:1332–44.
[30] Newman J, Thomas-Alyea KE, Thomas-Alyea KE. Electrochemical systems. Somerset, United States. Incorporated: John Wiley & Sons; 2012.
[31] Bazant M. 10.626 electrochemical energy systems. Spring: Massachusetts institute of Technology: MIT OpenCourseWare; 2014.
[32] Haverkort JW, Rajaei H. Voltage losses in zero-gap alkaline water electrolysis. J Power Sources 2021;497:229864.
[33] Haverkort JW. Modeling and experiments of binary electrolytesin the presence of diffusion, migration, and electro-osmotic flow. Phys Rev Appl 2020;14:044047.
[34] Haverkort JW, Rajaei H. Electro-Osmotic flow and the limiting current in alkaline water electrolysis. J Power Sour Advan 2020;6:100034.
[35] Falcão DS, Pinto AMFR. A review on PEM electrolyzer modelling: guidelines for beginners. J Clean Prod 2020;261:121184.
[36] Ursúa A, Sanchis P. Static-dynamic modelling of the electrical behaviour of a commercial advanced alkaline water electrolyser. Int J Hydrogen Energy 2012;37:18598–614.
[37] Ulleberg O. Modeling of advanced alkaline electrolyzers: a system simulation approach. Int J Hydrogen Energy 2003;28:21–33.
[38] Zenith F, Seland F, Kongstein OE, Børresen B, Tunold R, Skogestad S. Control-oriented modelling and experimental study of the transient response of a high-temperature polymer fuel cell. J Power Sources 2006;162:215–27.
[39] Immerz C, Bensmann B, Trinke P, Suermann M, Hanke-Rauschenbach R. Understanding electrical under- and overshoots in proton exchange membrane water electrolysis cells. J Electrochem Soc 2019;166:F1200–8.
[40] Maamouri R, Guilbert D, Zasadzinski M, Rafaralahy H. Proton exchange membrane water electrolysis: modeling for hydrogen flow rate control. Int J Hydrogen Energy 2021;46:7676–700.
[41] Niaz AK, Park JY, Lim HT. Operational parameters correlated with the long-term stability of anion exchange membrane water electrolyzers. Int J Hydrogen Energy 2021;46:31550–62.
[42] Randles JEB. Kinetics of rapid electrode reactions. Discuss Faraday Soc 1947;1:11–9.
[43] Rozain C, Millet P. Electrochemical characterization of polymer electrolyte membrane water electrolysis cells. Electrochim Acta 2014;131:160–7.
[44] Guilbert D, Vitale G. Dynamic emulation of a PEM electrolyzer by time constant based exponential model. Energies 2019;12.
[45] Van Der Merwe J, Uren K, Van Schoor G, Bessarabov D. A study of the loss characteristics of a single cell PEM electrolyser for pure hydrogen production. In: Proceedings of the IEEE international conference on industrial technology; 2013. p. 668–72.
[46] Martinson CA, van Schoor G, Uren KR, Bessarabov D. Characterisation of a PEM electrolyser using the current interrupt method. Int J Hydrogen Energy 2014;39:20865–78.
[47] Lopes FDC, Watanabe EH. Experimental and theoretical development of a PEM electrolyzer model applied to energy storage systems. In: Conference BPE, editor. Brazilian power electronics conference, COBEP2009: 2009 Brazilian power electronics conference; 2009. p. 775–82. 2009.
[48] Atlam O, Kolhe M. Equivalent electrical model for a proton exchange membrane (PEM) electrolyser. Energy Convers Manag 2011;52:2952–7.
[49] Milewski J, Guandalini G, Campanari S. Modeling an alkaline electrolysis cell through reduced-order and loss-estimate approaches. J Power Sources 2014;269:203–11.
[50] Górecki K, Zarębski J, Górecki P, Halbryt S. Modelling and the analysis of the power supply system for the generator of hydrogen. In: Oral AY, Bahsi Oral ZB, Ozer M, editors. 2nd international congress on energy efficiency and energy related materials (ENEFM2014). Cham: Springer International Publishing; 2015. p. 451–7.
[51] Górecki K, Górecki P, Zarębski J. Electrical model of the alkaline electrolyser dedicated for SPICE. Int J Circ Theor Appl 2018;46:1044–54.
[52] Henao C, Agbossou K, Hammoudi M, Dube Y, Cardenas A. Simulation tool based on a physics model and an electrical analogy for an alkaline electrolyser. J Power Sources 2014;250:58–67.
[53] LeRoy RL, Janjua MBI, Renaud R, Leuenberger U. Analysis of time-variation effects in water electrolyzers. J Electrochem Soc 1979;126:1674–82.
[54] Eichman J, Harrison K, Peters M. Novel electrolyzer applications: providing more than just hydrogen. United States; 2014.
[55] Sánchez M, Amores E, Rodríguez L, Clemente-Jul C. Semi-empirical model and experimental validation for the performance evaluation of a 15 kW alkaline water electrolyzer. Int J Hydrogen Energy 2018;43:20332–45.
[56] Lim A, Kim H-j, Henkensmeier D, Yoo SJ, Kim JY, Lee SY, et al. A study on fabrication and operation variables affecting the performance of anion exchange membrane water electrolysis. J Ind Eng Chem 2019;76:410–8.
[57] Shen X, Zhang X, Li G, Lie TT, Hong L. Experimental study on the external electrical thermal and dynamic power characteristics of alkaline water electrolyzer. Int J Energy Res 2018;42:3244–57.
[58] Trinke P, Haug P, Brauns J, Bensmann B, Hanke-Rauschenbach R, Turek T. Hydrogen crossover in PEM and alkaline water electrolysis: mechanisms, direct comparison and mitigation strategies. J Electrochem Soc 2018;165:F502–13.
[59] Ito H, Kawaguchi N, Someya S, Munakata T. Pressurized operation of anion exchange membrane water electrolysis. Electrochim Acta 2019;297:188–96.
[60] Ogumerem G, Pistikopoulos E. Dynamic modeling and explicit control of a PEM water electrolysis process. Smart Sustain Manufactur Syst 2018;2:25–43.
[61] Colbertaldo P, Gómez Aláez SL, Campanari S. Zero-dimensional dynamic modeling of PEM electrolyzers. In: International conference on applied energy. Cardiff, UK: Energy Procedia; 2017. p. 1468–73.
[62] Kiaee M, Cruden A, Chladek P, Infield D. Demonstration of the operation and performance of a pressurised alkaline electrolyser operating in the hydrogen fuelling station in Porsgrunn, Norway. Energy Convers Manag 2015;94:40–50.
[63] Stansberry JM, Brouwer J. Experimental dynamic dispatch of a 60 kW proton exchange membrane electrolyzer in power-to-gas application. Int J Hydrogen Energy 2020;45:9305–16.
[64] ENAPTER. AEM technology. Enapter handbook.
[65] Stansberry J, Hormaza Mejia A, Zhao L, Brouwer J. Experimental analysis of photovoltaic integration with a proton exchange membrane electrolysis system for power-to-gas. Int J Hydrogen Energy 2017;42:30569–83.
[66] SIEMENS. Silizer 300. The next paradigm of PEM electrolysis.
[67] Tuinema BW, Adabi E, Ayivor PKS, Suárez VG, Liu L, Perilla A, et al. Modelling of large-sized electrolysers for real-time simulation and study of the possibility of frequency support by electrolysers. IET Gener, Transm Distrib 2020;14:1985–92.
[68] Gorre J, Ruoss F, Karjunen H, Schaffert J, Tynjälä T. Cost benefits of optimizing hydrogen storage and methanation capacities for Power-to-Gas plants in dynamic operation. Appl Energy 2020:257.
[69] Chen C, Lu Y, Xing L. Levelling renewable power output using hydrogen-based storage systems: a techno-economic analysis. J Energy Storage 2021;37.
[70] Alshehri F, Suarez VG, Torres JLR, Perilla A, van der Meijden MAMM. Modelling and evaluation of PEM hydrogen technologies for frequency ancillary services in future multi-energy sustainable power systems. Heliyon 2019;5.

[71] Champion NREL. Photovoltaic module efficiency chart. 2022.
[72] Fereidooni M, Mostafaeipour A, Kalantar V, Goudarzi H. A comprehensive evaluation of hydrogen production from photovoltaiv power station. Renewable Sustainable Energy Rev 2018;82:415–23.
[73] Fopah-Lele A, Kabore-Kere A, Tamba JG, Yaya-Nadjo I. Solar electricity storage through green hydrogen production: a case study. Int J Energy Res 2021;45:13007–21.
[74] Reuß M, Reul J, Grube T, Langemann M, Calnan S, Robinius M, et al. Solar hydrogen production: a bottom-up analysis of different photovoltaic-electrolysis pathways. Sustain Energy Fuels 2019:801–13.
[75] Sayedin F, Maroufmashat A, Sattari S, Elkamel A, Fowler M. Optimization of Photovoltaic Electrolyzer hybrid systems; taking into account the effect of climate conditions. Energy Convers Manag 2016;118:438–49.
[76] Duc TN, Goshome K, Endo N, Maeda T. Optimization strategy for high efficiency 20 kW-class direct coupled photovoltaic-electrolyzer system based on experimental data. Int J Hydrogen Energy 2019;44:26741–52.
[77] Topriska E, Kolokotroni M, Dehouche Z, Potopsingh R, Wilson E. The application of solar-powered polymer electrolyte membrane (PEM) electrolysers for the sustainable production of hydrogen gas as a fuel for domestic cooking. In: Sayigh A, editor. Renewable energy in the service of mankind Vol I. Cham: Springer; 2015. p. 193–203.
[78] Vaculik J, Hradilek Z, Moldrik P, Minarik D. Calculation of the efficiency of hydrogen storage system at the fuel cells laboratory. In: 15th International scientific conference on electrical power engineering (EPE). Brno-Bystrc. Czech Republic: IEEE; 2014. p. 381–4. 2014.
[79] Rahim AHA, Tijani AS, Fadhullah M, Hanapi S, Sainan KI. Optimization of direct coupling solar PV panel and advanced alkaline electrolyzer system. Energy Proc 2015;79:204–11.
[80] Badea G, Naghiu GS, Giurca I, Aşchilean I, Megyesi E. Hydrogen production using solar energy - technical analysis. Energy Proc 2017;112:418–25.
[81] Khalilnejad A, Sundararajan A, Sarwat A. Performance evaluation of optimal photovoltaic-electrolyzer system with the purpose of maximum Hydrogen storage. In: IEEE/IAS 52nd industrial and commercial power systems technical conference (I&CPS); 2016. p. 1–9. 2016.
[82] Węcel D, Jurczyk M, Uchman W, Skorek-Osikowska A. Investigation on system for renewable electricity storage in small scale integrating photovoltaics, batteries, and hydrogen generator. Energies 2020;13:6039.
[83] Laoun B, Khellaf A, Naceur MW, Kannan AM. Modeling of solar photovoltaic-polymer electrolyte membrane electrolyzer direct oupling for hydrogen generation. Int J Hydrogen Energy 2016;41:10120–35.
[84] Su Z, Ding S, Gan Z, Yang X. Optimization and sensitivity analysis of a photovoltaic-electrolyser direct-coupling system in Beijing. Int J Hydrogen Energy 2014;39:7202–15.
[85] Ferrari ML, Rivarolo M, Massardo AF. Hydrogen production system from photovoltaic panels: experimental characterization and size optimization. Energy Convers Manag 2016;116:194–202.
[86] Bhattacharyya R, Misra A, Sandeep KC. Photovoltaic solar energy conversion for hydrogen production by alkaline water electrolysis: conceptual design and analysis. Energy Convers Manag 2017;133:1–13.
[87] Niaz H, Lakouraj MM, Liu J. Techno-economic feasibility evaluation of a standalone solar-powered alkaline water electrolyzer considering the influence of battery energy storage system: a Korean case study. Kor J Chem Eng 2021;38:1617–30.
[88] Privitera SMS, Muller M, Zwaygardt W, Carmo M, Milazzo RG, Zani P, et al. Highly efficient solar hydrogen production through the use of bifacial photovoltaics and membrane electrolysis. J Power Sources 2020;473:228619.
[89] Gutiérrez-Martín F, Amodio L, Pagano M. Hydrogen production by water electrolysis and off-grid solar PV. Int J Hydrogen Energy 2020.
[90] Phap VM, Sang LQ, Ninh NQ, Binh DV, Hung BB, Huyen CTT, et al. Feasibility analysis of hydrogen production potential from rooftop solar power plant for industrial zones in Vietnam. Energy Rep 2022;8:14089–101.
[91] Mas R, Berastain A, Antoniou A, Angeles L, Valencia S, Celis C. Genetic algorithms-based size optimization of directly and indirectly coupled photovoltaic-electrolyzer systems. Energy Convers Manag 2022;270:116213.
[92] Butt OM, Saeed T, Elahi H, Masud U, Ghafoor U, Che HS, et al. A predictive approach to optimize a HHO generator coupled with solar PV as a standalone system. Sustainability 2021;13:12110.
[93] Yang Z, Lin J, Zhang H, Lin B, Lin G. A new direct coupling method for photovoltaic module-PEM electrolyzer stack for hydrogen production. Fuel Cell 2018;18:543–50.
[94] Frites M, Khan SUM. Optimum conditions for efficient hydrogen production generation by water electrolysis in an electrochemical cell powered either by power supply or solar cells. ECS Trans 2013;50:3.
[95] Ganjehsarabi H. Performance assessmen of solar-powered high pressure proton exchange membrane electrolyzer: a case study for Erzincan. Int J Hydrogen Energy 2019;44:9701–7.
[96] Argonne National Laboratory. Basic research needs for the hydrogen economy. 2003.
[97] Office of energy efficiency & renewable energy. Hydrogen and fuel cell technologies office multi-year research, development and demonstration plan. US Department of Energy; 2014.
[98] Wijayatha KGU. Photoelectrochemical cells for hydrogen generation. In: Kilner JA, Skinner SJ, Irvine SJC, Edwards PP, editors. Functional materials for sustainable energy applications. Woodhead Publishing; 2012. 91–146e.
[99] Kelly NA. The coupling factor: a new metric for determining and controlling the efficiency of solar photovoltaic power utilization. Int J Hydrogen Energy 2013;38:2079–94.
[100] García-Valverde R, Espinosa N, Urbina A. Optimized method for photovoltaic-water electrolyser direct coupling. Int J Hydrogen Energy 2011;36:10574–86.
[101] Shriyan NR. Modelling of PV-Electrolyzer system for optimum operation. Delft University of Technology; 2020.
[102] Tao M, Azzolini JA, Stechel EB, Ayers KE, Valdez TI. Review-engineering challenges in green hydrogen production systems. J Electrochem Soc 2022;169:054503.
[103] Siriramagiri GM, Luc W, Jiao F, Ayers K, Dobson KD, Hegedus SS. Computation and assessment of solar electrolyzer field performance: comparing coupling strategies. Sustain Energy Fuels 2019;3:422–30.
[104] System advisor model.
[105] Guilbert D, Collura SM, Scipioni A. DC/DC converter topologies for electrolyzers: state-of-the-art and remaining key issues. Int J Hydrogen Energy 2017;42:23966–85.
[106] Becker M, Brauns J, Turek T. Battery-buffered alkaline water electrolysis powered by photovoltaics. Chem Ing Tech 2021;93:655–63.
[107] Gillesen B, Heinrichs HU, Stenzel P, Linssen J. Hybridization strategies of power-to-gas systems and battery storage using renewable energy. Int J Hydrogen Energy 2017;42:13554–67.
[108] Papadopoulos V, Desmet J, Knockaert J, Develder C. Improving the utilization factor of a PEM electrolyzer powered by a 15 MW PV park by combining wind power and battery storage - feasibility study. Int J Hydrogen Energy 2018;43:16468–78.
[109] Koyama M. Toward economically rational hydrogen production from solar energy: from battery versus hydrogen to battery × hydrogen. In: Atesin T, Bashir S, Liu J, editors. Nanostructured materials for next-generation energy storage and conversion. Berlin, Heidelberg: Springer; 2019.
[110] Sako N, Koyama M, Okubo T, Kikuchi Y. Techno-economic and life cycle analyses of battery-assisted hydrogen production systems from photovoltaic power. J Clean Prod 2021;298:126809.
[111] Lee CH, Lee JK, Zhao B, Fahy KF, Bazylak A. Transient gas saturation in porous transport layers of polymer electrolyte membrane electrolyzers. ECS Trans 2019;8:821–32. ed.
[112] Schnuelle C, Wassermann T, Fuhrlaender D, Zondervan E. Dynamic hydrogen production from PV & wind direct electricity supply – modeling and techno-economic assessment. Int J Hydrogen Energy 2020;45:29938–52.
[113] Brauns J, Turek T. Alkaline water electrolysis powered by renewable energy: a review. Processes 2020;8.
[114] Dobo Z, Palotas AB. Impact of the current fluctuation on the efficiency of alkaline water electrolysis. Int J Hydrogen Energy 2017;42:5649–56.
[115] Dobó Z, Palotás ÁB. Impact of the voltage fluctuation of the power supply on the efficiency of alkaline water electrolysis. Int J Hydrogen Energy 2016;41:11849–56.
[116] Speckmann FW, Bintz S, Groninger ML, Birke KP. Alkaline electrolysis with overpotential-reducing current profiles. J Electrochem Soc 2018;165:F456–62.
[117] Allidières L, Brisse A, Millet P, Valentin S, Zeller M. On the ability of pem water electrolysers to provide power grid services. Int J Hydrogen Energy 2019;44:9690–700.
[118] Furfari S, Clerici A. Green hydrogen: the crucial performance of electrolysers fed by variable and intermittent renewable electricity. Europ Phys J Plus 2021:136.
[119] Fischer D, Kaufmann F, Hollinger R, Voglstätter C. Real live demonstration of MPC for a power-to-gas plant. Appl Energy 2018;228:833–42.
[120] Ewan M, Rocheleau R, Swider-Lyons KE, Devlin P, Virji M, Randolf G. Development of a hydrogen energy system as a grid frequency management tool. ECS Trans 2016;14:403–19. ed.
[121] Bergen A, Pitt L, Rowe A, Wild P, Djilali N. Transient electrolyser response in a renewable-regenerative energy system. Int J Hydrogen Energy 2009;34:64–70.
[122] Schmidt O, Gambhir A, Staffell I, Hawkes A, Nelson J, Few S. Future cost and performance of water electrolysis: an expert elicitation study. Int J Hydrogen Energy 2017;42:30470–92.
[123] Wu JF, Yuan XZ, Martin JJ, Wang HJ, Zhang JJ, Shen J, et al. A review of PEM fuel cell durability: degradation mechanisms and mitigation strategies. J Power Sources 2008;184:104–19.
[124] Feng Q, Yuan XZ, Liu GY, Wei B, Zhang Z, Li H, et al. A review of proton exchange membrane water electrolysis on degradation mechanisms and mitigation strategies. J Power Sources 2017;366:33–55.
[125] Rakousky C, Reimer U, Wippermann K, Kuhri S, Carmo M, Lueke W, et al. Polymer electrolyte membrane water electrolysis: restraining degradation in the presence of fluctuating power. J Power Sources 2017;342:38–47.
[126] Weiß A, Siebel A, Bernt M, Shen T-H, Tileli V, Gasteiger H. Impact of intermittent operation on lifetime and performance of a PEM water electrolyzer. J Electrochem Soc 2019;166:F487–97.
[127] Grigoriev SA, Bessarabov DG, Fateev VN. Degradation mechanisms of MEA characteristics during water electrolysis in solid polymer electrolyte cells. Russ J Electrochem 2017;53:318–23.
[128] Aßmann P, Gago AS, Gazdzicki P, Friedrich KA, Wark M. Toward developing accelerated stress tests for proton exchange membrane electrolyzers. Curr Opinion Electrochem 2020;21:225–33.
[129] Uchino Y, Kobayashi T, Hasegawa S, Nagashima I, Sunada Y, Manabe A, et al. Relationship between the redox reactions on a bipolar plate and reverse current after alkaline water electrolysis. Electrocatalysis 2018;9:67–74.

[130] Niaz AK, Akhtar A, Park JY, Lim HT. Effects of the operation mode on the degradation behavior of anion exchange membrane water electrolyzers. J Power Sources 2021:481.
[131] Stucki S, Scherer GG, Schlagowski S, Fischer E. PEM water electrolysers: evidence for membrane failure in 100 kW demonstration plants. J Appl Electrochem 1998; 28:1041–9.
[132] Chandesris M, Medeau V, Guillet N, Chelghoum S, Thoby D, Fouda-Onana F. Membrane degradation in PEM water electrolyzer: numerical modeling and experimental evidence of the influence of temperature and current density. Int J Hydrogen Energy 2015;40:1353–66.
[133] Millet P, Ranjbari A, de Guglielmo F, Grigoriev SA, Aupretre F. Cell failure mechanisms in PEM water electrolyzers. Int J Hydrogen Energy 2012;37: 17478–87.
[134] Lettenmeier P, Wang R, Abouatallah R, Burggraf F, Gago AS, Friedrich KA. Proton exchange membrane electrolyzer systems operating dynamically at high current densities. ECS Trans 2016;23:11–21. ed.